JOURNAL OF GEOPHYSICAL RESEARCH, VOL. 105, NO. E11, PAGES 26,695–26,711, NOVEMBER 25, 2000

Kilometer-scale roughness of Mars: Results from MOLA data analysis

Mikhail A. Kreslavsky

Astronomical Observatory, Kharkov University, Kharkov, Ukraine
Department of Geological Sciences, Brown University, Providence, Rhode Island

James W. Head III

Department of Geological Sciences, Brown University, Providence, Rhode Island

Abstract. The Mars Orbiter Laser Altimeter (MOLA) data are used to characterize the kilometer-scale surface roughness of Mars. The median absolute value of the differential slope at a given baseline is proposed as a data-derived measure of the surface roughness at this scale. Study of the scale dependence of roughness for the smoothest terrains gives an independent estimate of 20 cm for MOLA ranging accuracy. The baseline lengths from 0.6 to ~20 km are used, and kilometer-scale roughness is mapped for the entire surface. The maps show that different geological units have distinctive roughness characteristics. Scale dependence of roughness for a number of geological units is presented and discussed. The southern polar cap is rougher than the northern at kilometer and subkilometer scale, which suggests differences in the sublimation/condensation balance. The Vastitas Borealis Formation has a distinctive 3-km-scale background surface topography, which suggests a nonvolcanic origin for its upper layer. Young volcanic plains in Amazonis Planitia and the eastern part of Elysium Planitia are very similar to each other in their roughness characteristics and differ from other volcanic plains on Mars, which suggests a distinctive eruption style. There are systematic latitudinal variations of roughness in both the southern highlands and the northern lowlands: terrains at high latitude are smoother at short baselines; the characteristic vertical scale related to this difference is several meters. Processes that could be responsible for formation of this trend include creep of ice-rich near-surface material at high latitudes, treatment of the surface with repetitive deposition and sublimation of seasonal frost, climate-controlled deposition and/or cementation of dust at high latitudes, and repetitive sublimation and accumulation of subsurface ice at low latitudes with climate variations. All mechanisms of origin could operate more effectively under different climate conditions. Relevant morphological observations favor mechanisms involving deposition of smooth blankets at high latitudes.

1. Introduction

The Mars Orbiter Laser Altimeter (MOLA) [*Zuber et al.*, 1992] on board the Mars Global Surveyor (MGS) [*Albee et al.*, 1998] covered the surface of Mars with a dense network of precise measurements of surface elevation [*Smith et al.*, 1998, 1999]. Topographic maps of Mars produced with these data [*Smith et al.*, 1999] have a spatial resolution of ~4 km. MOLA shot spacing along track is ~0.3 km, noticeably shorter than the maximal spacing between tracks. Hence any algorithm used to produce interpolated topographic maps inevitably omits some information from the data set. Working with individual profiles allows researchers to achieve the maximal resolution but limits the ability to gain an overview of all the data. On the other hand, statistical analysis of topographic variations along profiles allows one both to exploit the highest resolution of the data and to obtain a global overview.

Aharonson et al. [1998, 1999] and *Smith et al.* [1999] have used the interquartile scale of topography at a 100-km-long baseline to characterize surface roughness and produced global maps portraying 100-km-scale topography variations. *Malamud and Turcotte* [2000] used wavelet analysis to characterize the topography for several segments of MOLA profiles. *Garneau and Plaut* [2000] studied the scale dependence of the RMS slope for several MOLA profiles, applying the ideas of fractal statistics.

In our previous work [*Kreslavsky and Head*, 1999] we have used MOLA profiles from initial phases of the mission to study the roughness of the Martian surface and its scale dependence in the scale range from hundreds of meters to tens of kilometers. We have found the distinctive characteristic 3-km-scale roughness of the Vastitas Borealis Formation and noted the remarkable smoothness of the north polar cap surface at small scale. In that study we used the median absolute values of slope as a measure of roughness. The major shortcoming of that approach is that the median absolute value of slope actually is a mixture of the true surface roughness and regional slopes [*Kreslavsky and Head*, 1999]. In the present study we use a new, and in some ways better, measure of roughness, free from this major shortcoming. We apply this new approach to global data coverage from the nominal mission.

In this paper we first describe in detail our roughness characterization technique. Then we present roughness maps and

Paper number 2000JE001259.
0148-0227/00/2000JE001259$09.00

show some instructive examples of scale dependences of roughness for several terrains. Then we discuss a newly identified latitudinal trend of roughness. Preliminary results of this study have been reported [*Kreslavsky and Head*, 2000a, 2000b; *Head and Kreslavsky*, 2000].

2. Characterization of Surface Roughness

2.1. Measure of Roughness: Median Differential Slope

Surface slope at some baseline is generally defined by a set of features with horizontal scales of order of the baseline length or larger, including regional slopes. To characterize intrinsic surface roughness at a given scale, we need to exclude slopes due to larger features and preserve only slopes due to features of the baseline scale. Here we propose to do this in the following way. For each data point we take two points a half baseline ahead and half baseline behind (Figure 1). We calculate the (signed) elevation difference between these points. Then we calculate the (signed) elevation difference for a baseline that is twice as long, taking points one baseline ahead and one baseline behind. We subtract half of the latter difference from the former difference. In this way we remove larger-scale tilt from the elevation difference at a given baseline. This corrected elevation difference divided by the baseline length can be considered as the tangent of some slope, which we call "the differential slope." The differential slope at a given point is close to the angle shown in Figure 1, unless slopes are very steep.

Let h_x be the elevation at the distance x from a given point and let l be the baseline length. The differential slope α_l at this baseline at the given point is then defined with the equation

$$\tan(\alpha) = \frac{\left(h_{l/2} - h_{-l/2}\right) - \frac{1}{2}\left(h_l - h_{-l}\right)}{l}. \quad (1)$$

Equation (1) introduces a linear band-pass filter. Its transfer function is proportional to

$$F(k) = \frac{1}{l}\left(2\sin\frac{kl}{2} - \sin kl\right), \quad (2)$$

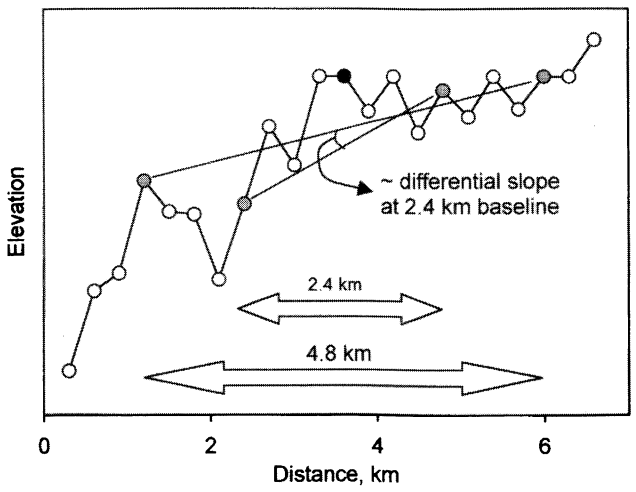

Figure 1. Scheme showing definition of the differential slope. The differential slope at the profile point marked with black is calculated using elevations of four points marked with gray.

where k is the wavenumber. The peak of the band is at $k_l = \frac{4}{3}\pi l^{-1}$, that is, at the wavelength of $\frac{3}{2}l$. The band extends at the level of 1/2 from $0.60k_l$ to $1.34k_l$.

The wavelet analysis performed by *Malamud and Turcotte* [2000] actually introduces another linear band-pass filter. It provides a somewhat narrower band and suppressed secondary bands, which is better for robust roughness characterization. However, this approach has two essential shortcomings in comparison to the approach we use. First, the wavelet analysis involves a large number of shots into calculations for each point, which makes it more sensitive to shots missing and hence less practical. Second, shots much farther than the effective baseline are involved, which reduces the effective along-track resolution and distorts sharp margins between terrains with different roughness.

A typical value of the differential slope for a specific area can be used as a characteristic of roughness. Here we use the median absolute value of the differential slope as such a quantity characterizing roughness. The advantages of using median absolute value rather than mean absolute value or RMS are related to the fact that the slope-frequency distribution, and hence differential-slope-frequency distribution, has long tails. These issues were discussed in detail by *Kreslavsky and Head* [1999].

2.2. Data Processing

We calculated the differential slopes at a hierarchy of baselines of 2, 4, 8, 16, 32, and 64 point-to-point distances, that is, for 0.6-, 1.2-, 2.4-, 4.8-, 9.6-, 19.2-km baseline lengths. For this study we used the whole set of data obtained during an early part of regular mapping within the period from March 1 to April 15, 1999 [*Smith et al.*, 1999] (~28 million shots). We carefully excluded all data with any irregularity of point spacing and spacecraft attitude.

We obtained maps of roughness calculating the median slope for all shots within each resolution cell of the map. We created the maps at 4-cells-per-degree resolution. If a cell contained fewer than 50 data points, we considered this cell as containing no data. If we decrease the minimal number of data points per cell, the noise increases, while when we increase the threshold, the gaps in coverage increase. Then all gaps with no data (~40% of all cells) were filled with values from neighboring cells. Usually, the gap widths were 1-2 cells, in rare cases up to 7 cells. We found that locally incorporating some data obtained later in the mission into the analysis does not bring apparent improvement of the maps at this resolution.

We also calculated the median differential slopes for a number of regions and geological units in a way similar to that used in our previous work [*Kreslavsky and Head*, 1999]. To avoid any errors in coregistering of digitized geological maps [*Scott and Tanaka*, 1986; *Tanaka and Scott*, 1987; *Greeley and Guest*, 1987] and MOLA data, we excluded all shots close to the unit boundaries.

Note that the roughness was measured only along MOLA passes. Absolute accuracy of MOLA measurements and pass-to-pass spacing are not good enough to perform the same analysis in the cross-track direction.

3. Overview of Kilometer-Scale Surface Roughness on Mars

The maps of roughness are presented in Plate 1 in simple cylindrical projection and Plate 2 in Lambert azimuthal projec-

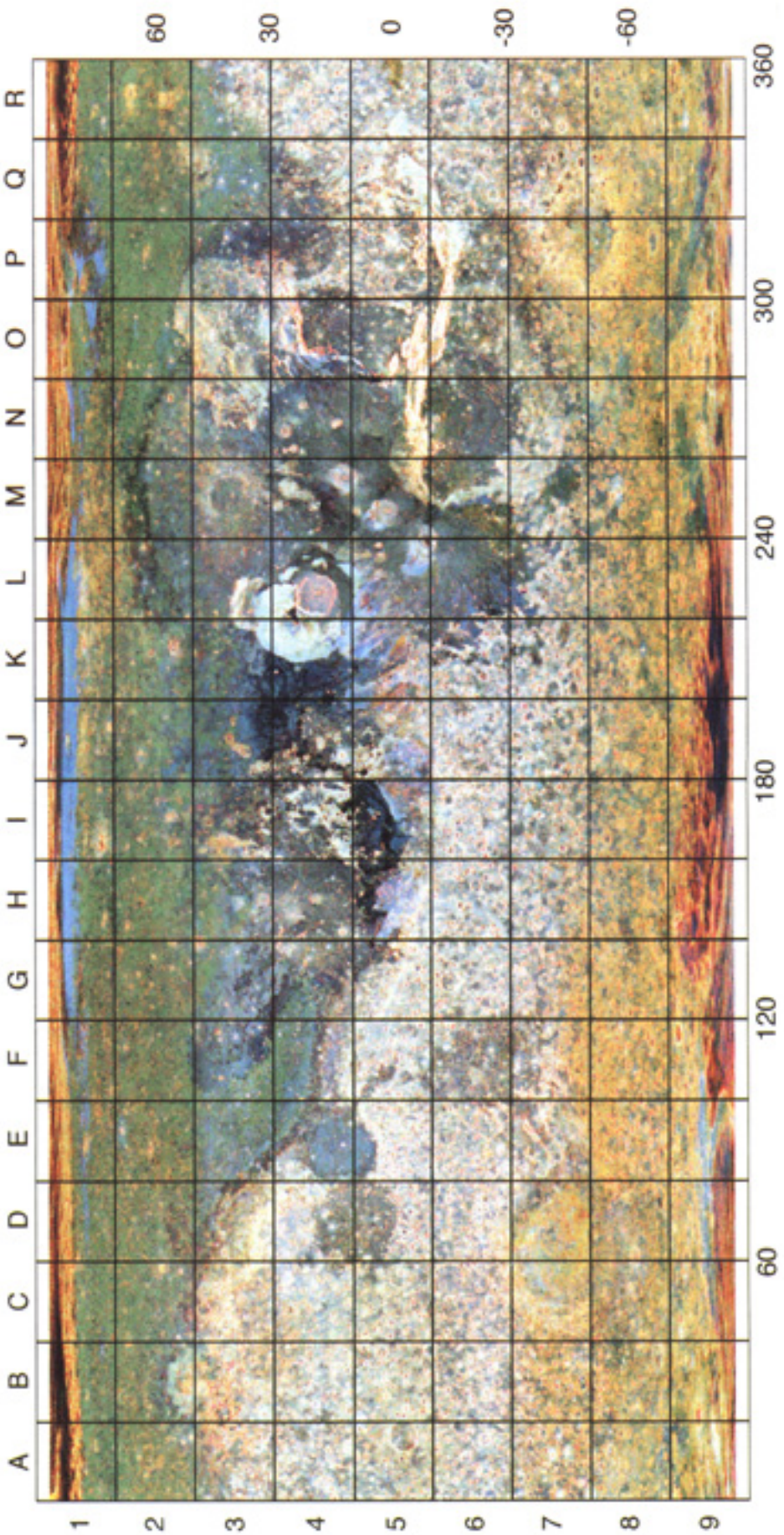

Plate 1. Map of kilometer-scale surface roughness of Mars. Map projection is simple cylindrical. The map is a composite RGB image. The median absolute values of the differential slopes at 0.6-, 2.4-, and 19.2-km baselines are used as the blue, green, and red channels, respectively. Brighter shades denote a rougher surface.

tion for both the northern and southern hemispheres. The maps are presented as three-color RGB composites. The red channel codes the median absolute values of differential slope at the longest (19.2-km) baseline. Brighter shades denote higher roughness values. In the same way, the green channel codes the intermediate-scale roughness (2.4-km baseline length), and the blue channel codes the smallest-scale roughness (0.6-km baseline length). For each baseline used, the median differential slope varies over the Martian surface in a range exceeding 2 orders of magnitude.

The Martian dichotomy boundary is clearly seen in the roughness map (Plate 1) as a boundary between smoother (darker in the map) northern lowlands and rougher (brighter) highlands. Numerous rough (bright) spots in the lowlands (Plate 2a) are usually related to large impact craters. The greatest scarps are seen in the maps as bright red and orange outline (as a narrow band of very high large-scale roughness), for example, the Olympus Mons scarps (Plate 1, box L4), the walls of Valles Marineris (N5, O5, O6, P6), and the southern wall of Kasei Valles (O4). Large expanses of volcanic plains are generally smoother (darker in the map) and are clearly seen amid the rough cratered highland surface, for example, Syrtis Major (D4, D5) and Hesperia Planum (F6). Generally, most volcanic plains display similar roughness at all scales (gray in the map), but some differences in roughness characteristics (shades of gray) between different volcanic units are seen, for example, in Dedalia Planum (L6). Many sharp boundaries between areas of contrasting roughness characteristics (contrasting colors in the map) perfectly coincide with the boundaries of geologic units [*Scott and Tanaka*, 1986; *Tanaka and Scott*, 1987; *Greeley and Guest*, 1987], for example, boundaries between rough aureole members of the Olympus Mons Formation and much smoother plains members of this formation (L4 in Plate 1). Some discrepancies and boundaries not shown in the geological maps are the subject of a separate study.

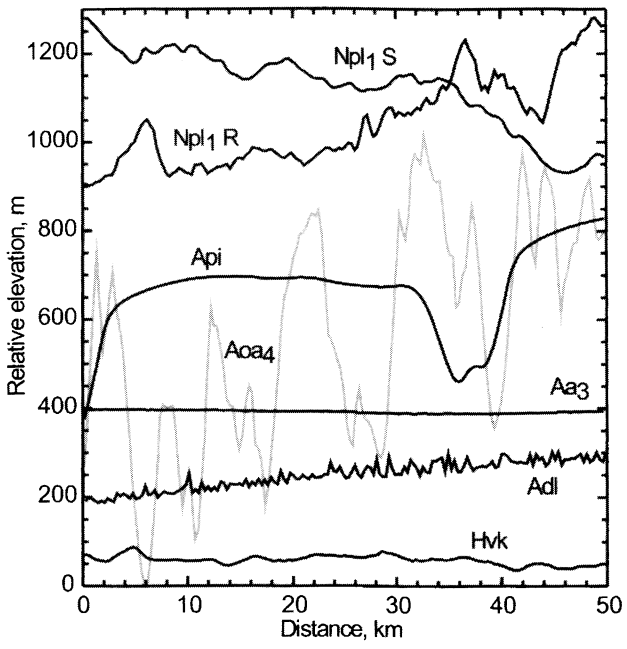

Figure 2. Typical segments of MOLA profiles for some geological units illustrating the diversity of kilometer-scale roughness: Api, the north polar cap, orbit 10226, 86°N, 24°E; Adl, linear dunes in Olympia Planitia, orbit 10225, 81°N, 166°E; Aa_3, the smooth member of the Arcadia Formation in Amazonis Planitia, orbit 10187, 29°N, 196°E; Hvk, the Knobby Member of the Vastitas Borealis Formation, orbit 10211, 65°N, 50°E; Aoa_4, the upper member of Olympus Mons Aureole, orbit 10224, 29°N, 217°E; Npl_1R, highland plateau at low latitude, orbit 10200, 20°S, 195°E; Npl_1S, highland plateau at high south latitude, orbit 10175, 58°S, 195°E. Profiles are arbitrarily shifted vertically.

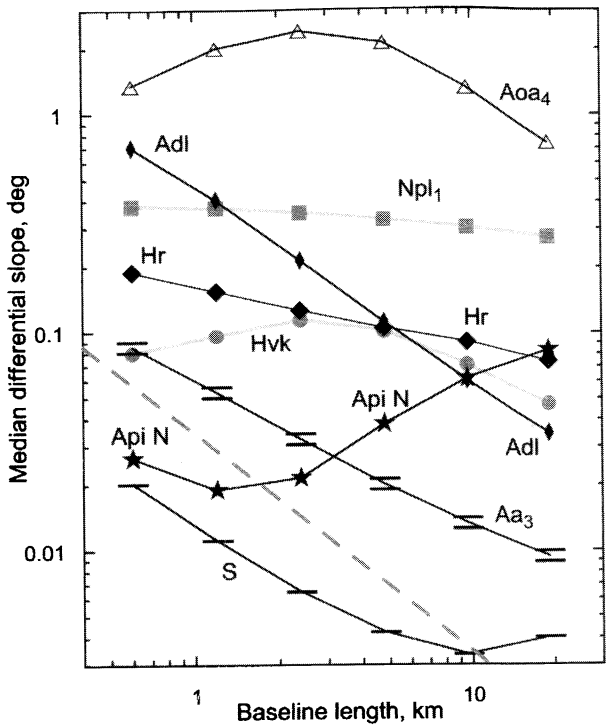

Figure 3. Dependence of the median differential slope on the baseline length for selected geological units illustrating the diversity of kilometer-scale roughness. Logarithmic scale on both axes. Api, the north polar cap; Apl, linear dunes; Aa_3, the smooth member of the Arcadia Formation; Hvk, the Knobby Member of the Vastitas Borealis Formation; Hr, ridged plain in Lunae Planum; Aoa_4, the upper member of Olympus Mons Aureole; Npl_1, highland plateau (cratered unit) in the latitudinal zone 25°-30°S; S, the smoothest area in the north polar cap. The dashed line shows the limit of MOLA measurement accuracy. Its inclination corresponds to the exponent of -1 for a power law dependence of roughness on scale.

Below, we consider some instructive examples of Martian terrains that display both marginal and typical roughness characteristics, present some typical MOLA profiles chosen from these terrains (Figure 2), and show the corresponding scale dependences of roughness (Figure 3). Note that when we chose the 50-km (~165 shots) segments of MOLA profiles shown in Figure 2, we did our best to show a typical profile reflecting the typical topography pattern of each terrain. However, we do not state that all surfaces of the given terrain have similar topography. To calculate the scale dependence of roughness in Figure 3, we used all shots (usually tens to hundreds of thousands) within the corresponding geological unit.

3.1. Olympus Mons Aureole

The roughest terrain on Mars is the upper member of Olympus Mons aureole deposits (denoted as Aoa_4 in Figures 2 and 3 according to the geologic map by *Scott and Tanaka* [1986]). These deposits are thought to be formed because of

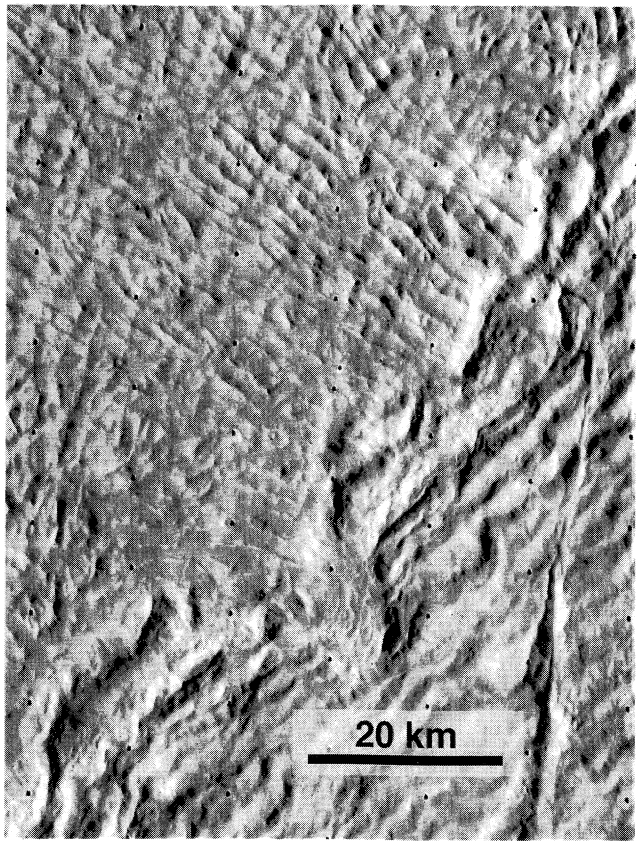

Figure 4. Viking high-resolution image 045B01 showing a part of the Olympus Mons aureole deposits. The scene is centered at 30.0°N, 214.2°E, north is approximately at the top. The upper member (Aoa_4 according to *Scott and Tanaka* [1986]) occupies the lower right half of the image, and the lower member (Aoa_1) occupies the upper left half.

gravitational movement of Olympus Mons material [e.g., *Francis and Wadge*, 1983; *Tanaka*, 1985]. The roughness is high at all scales, though the dependence of roughness on scale (Figure 3) has a well-pronounced maximum at ~2.5-km baseline length. In the roughness map (Plate 1, box K4), high roughness is coded with high intensity in all three channels, somewhat higher in blue and especially green, and somewhat lower in red; these give a bright cyan shade on the map.

The maximum in the scale dependence of roughness indicates that there is a characteristic scale of roughness for this terrain. This characteristic scale is well seen in the Viking images of this terrain (Figure 4, right) as the typical half-size of blocks forming the aureole. Note that the blocks often have a predominant orientation, which can lead to a bias in the estimation of typical block size from the scale dependence of roughness, when MOLA passes are oriented parallel to the block elongation. In a wide equatorial zone (including the region of Olympus Mons) the passes are oriented at ~8° to both sides of the north direction.

Members of Olympus Mons aureole deposits differ in their roughness (Figure 5). The lower member (Aoa_1) is essentially smoother, especially at larger scales, and has a shorter characteristic spatial scale of topography (position of the maximum in Figure 5). This difference is clearly seen in images of these terrains (Figure 4). At long baselines the median differential slope decreases as the power law with the exponent of approximately -0.8, rather close to the limiting case -1, which would mean the absolute absence of large-scale features. Thus the aureole has little topography at scales larger than the scale of blocks.

3.2. Highland Plateau

The profile marked as Npl_1 R in Figure 2 was chosen from a typical heavily cratered highland plateau in the equatorial region (specifically, from box J6, Plate 1). This example does not show the high steep topographical steps related to numerous crater walls, which are typical for the highlands. Such steps sometimes exceed the vertical extent of the plot in Figure 2, but they do not dominate the roughness values, especially for short baselines. Figure 3 (curve Npl_1) shows that the equatorial highland plateau is rather rough and shows little dependence of roughness on scale. This means that the topography of highlands is contributed by the whole spectrum of feature sizes in the scale range considered. Highlands are bright and spotty in the roughness map (Plate 1). This spotty pattern is controlled by abundant large craters with smoother floors and rougher walls.

3.3. Dunes

Linear transverse dunes around the north polar cap, mostly in Olympia Planitia (~80°N, 120°–240°E), are very rough at small scales and much smoother at large scales (Adl, Figures 2 and 3; image in Figure 6). In the roughness map (Plate 1, boxes G1-L1, Plate 2a), high small-scale roughness means a high intensity of blue color in the composite; lower roughness at longer baselines means a small admixture of green and almost no red. The resulting shade is bright blue.

The linear dependence of the median differential slope on the baseline length in the log-log plot (Figure 3) corresponds to a power law with exponent approximately -0.9, very close to -1. This indicates that there are almost no surface features of the scale of 1 km or larger in the region. The topography is almost entirely formed by features of <1 km size and spacing. This agrees with the dune spacing in the range of 0.3-0.8 km seen in the images [*Greeley et al.*, 1992] (Figure 6).

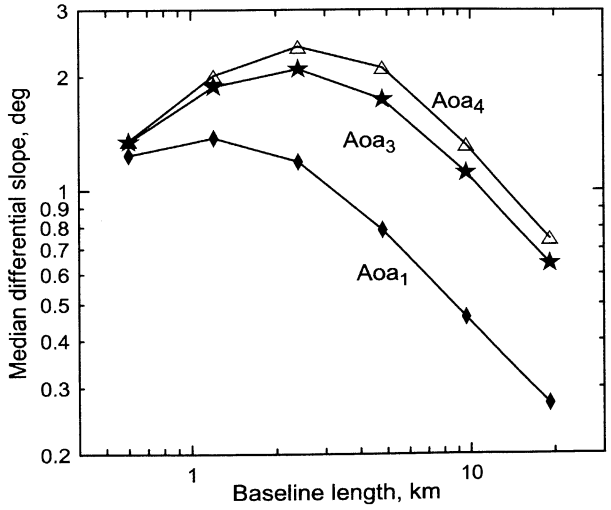

Figure 5. Dependence of the median differential slope on baseline length for Olympus Mons aureole. Logarithmic scale on both axes. The vertical scale is considerably stretched in comparison to Figure 3.

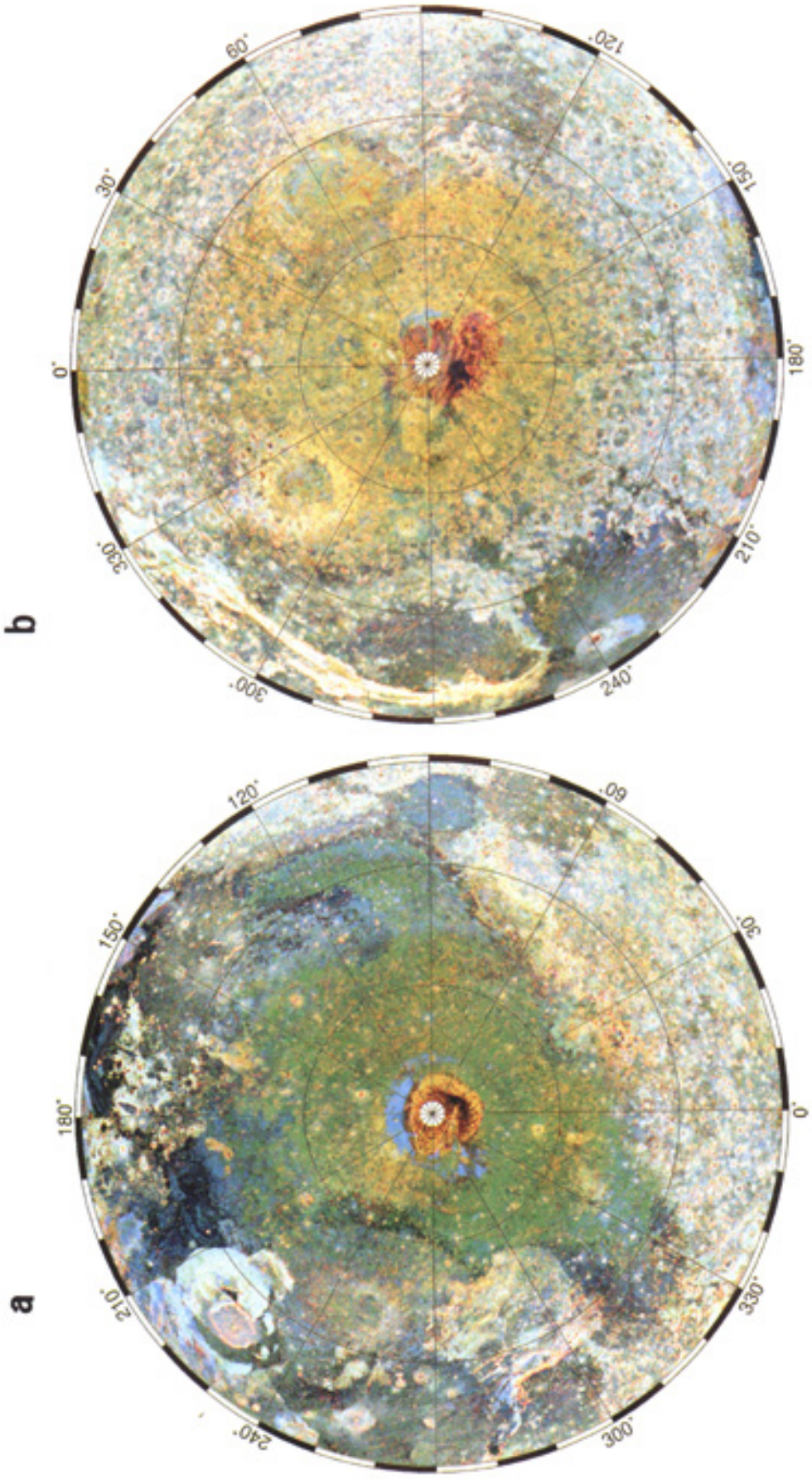

Plate 2. Map of kilometer-scale surface roughness of Mars. Map projection is polar Lambert azimuthal equal-area for the (a) northern and (b) southern hemispheres. Colors are the same as in Plate 1.

Note that the profiles of individual dunes are not sampled by MOLA, because the dunes are approximately of the same width as MOLA shot spacing; some aliasing occurs. Thus morphometric measurements of the dunes cannot be done directly from the MOLA profiles or digital elevation models. Linear dunes produce strongly anisotropic topography; hence statistical characteristics of profiles, including the median differential slope, depend on mutual orientation of passes and dunes. Variations of the small-scale roughness over Olympia Planitia (almost not seen in Plate 2a, but easily detectable in the digital version of the map) are not necessarily caused by variations of dune steepness, but can be controlled also by dune spacing and orientation. On the other hand, advanced statistical analysis of the profiles, if the spacing and orientation of the dunes are known from the images, promises accurate estimation of characteristic height and slopes of dunes despite aliasing.

3.4. Vastitas Borealis Formation

The Vastitas Borealis Formation [*Tanaka and Scott*, 1987] occupies a major part of the northern hemisphere of Mars. It is much smoother than highlands at all scales (profile Hvk in Figure 2 was taken from box C2, Plate 1). The scale dependence of roughness of the Vastitas Borealis Formation (e.g., the Knobby Member Hvk, Figure 3), displays a distinctive maximum at ~3-km baseline, which means that the topography is dominated by features with a characteristic horizontal scale of ~3 km. We have recognized this dominance of intermediate-scale topography from our study of initial MOLA data [*Kreslavsky and Head*, 1999]. The general smoothness means relatively dark shades in the roughness map; the dominance of the intermediate-scale roughness means relatively higher intensity in the green channel. As a result, the Vastitas Borealis Formation is deep green in the map (Plates 1 and 2a).

Typical differential slopes of the Vastitas Borealis Formation surface are ~0.15°. These differential slopes give ~0.3° characteristic slope of the characteristic 3-km features [*Kreslavsky and Head*, 1999]. Such gentle slopes are almost unrecognizable in Viking high-resolution images. In several regions, surface deposits of albedo-contrast material reveal this gentle topography in the images (Figure 7).

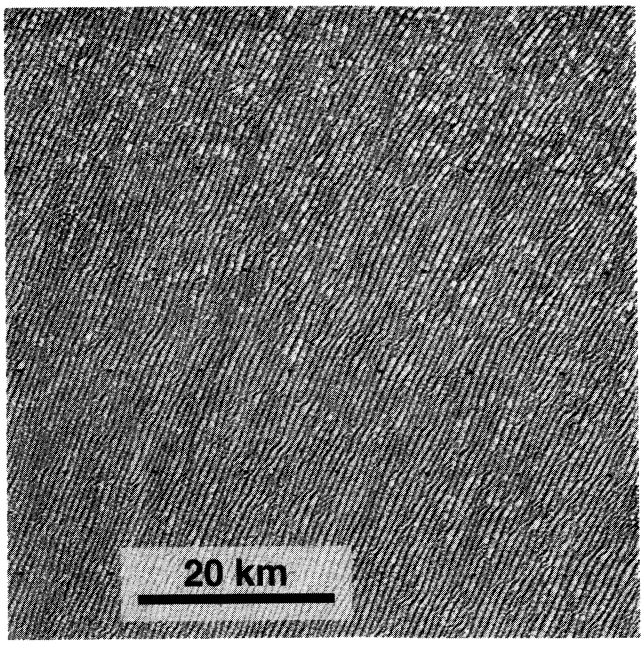

Figure 6. Viking high-resolution image 059B32 showing a small part of Olympia Planitia covered with linear dunes. The scene is centered at 81.3°N, 213.3°E; north is approximately at the top.

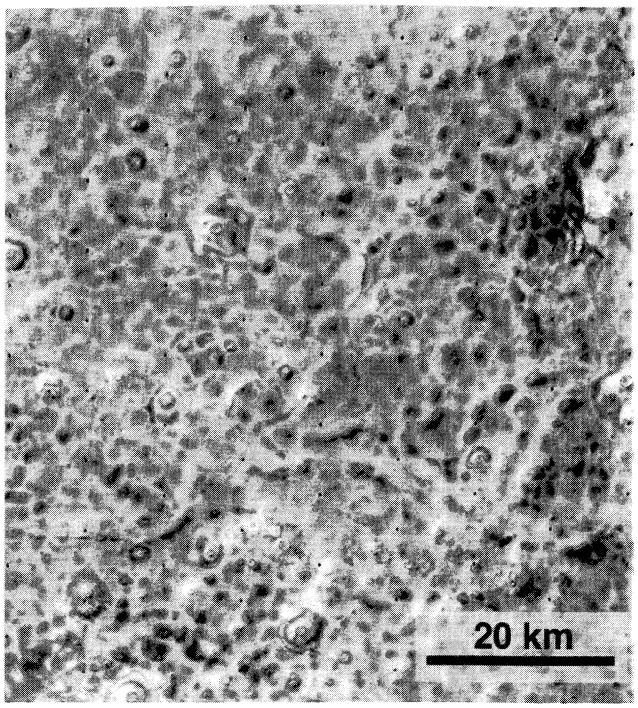

Figure 7. Viking high-resolution image 570B02 showing a small part of Vastitas Borealis, where some optically contrasting deposits highlight the gentle background topography. The scene is centered at 72.7°N, 89.8°E; north is approximately at the top.

The power law exponent for the scale dependence of roughness at long baselines (inclination of the right part of the Hvk curve in the log-log plot, Figure 3) is -0.55. It is noticeably different from the -1, which would occur if there were no features of large scale. This means that the background topography also includes some topographic features of scales larger than 3 km. Knobs, which are typical of the Vastitas Borealis Formation and especially the Knobby Member, are features of such scales (3-10 km) and contribute to roughness at this scale.

The four members of the Vastitas Borealis Formation, although varying in areal and altitude distributions [*Head and Kreslavsky*, 2000], display remarkably similar roughness characteristics. Their boundaries are hardly distinguishable in the roughness map (Plate 2a). The scale dependence of roughness (Figure 8) is similar for all members. The maximal difference between units (~2 times at the shortest baseline) is much smaller than the amplitude of roughness variations over the whole surface (~100 times at each baseline; note the difference in vertical scales in Figures 9 and 3). All members are characterized by the distinctive 3-km scale of surface slopes and very similar typical slopes at longer baselines, although the defending characteristics of the subunits (small knobs, ridges, groves, and albedo mottling) clearly differ. This suggests the same origin of the gentle background topography.

The Knobby Member (Hvk) and Mottled Member (Hvm) have the same roughness at all scales. The topography of these Vastitas Borealis Formation members may therefore be of the

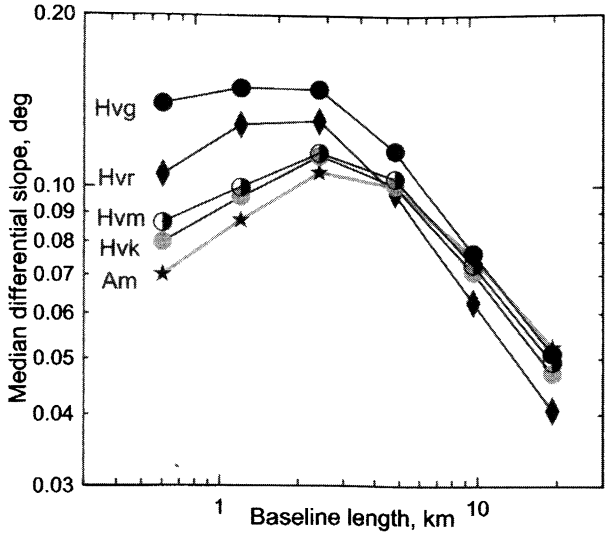

Figure 8. Dependence of the median differential slope on baseline length for the five geological units of northern plains. Am, circumpolar mantling deposits. Vastitas Borealis Formation members: Hvk, knobby; Hvm, mottled; Hvg, grooved; Hvr, ridged. Logarithmic scale on both axes. The vertical scale is considerably stretched in comparison to Figure 3.

same origin, and the characteristic albedo pattern of mottled terrains is formed by thin deposits, which are not seen in topography. Also shown in Figure 8 is the scale dependence of roughness for the circumpolar mantling deposits (Am). These young [*Tanaka and Scott*, 1987] deposits display the same scale dependence of roughness as Hvk and Hvm. This similarity suggests that much younger Am surface may be composed of the same type of material as the older Vastitas Borealis Formation and formed later by similar processes [*Kreslavsky and Head*, 1999].

The Grooved Member (Hvg) and the Ridged Member (Hvr) have higher roughness at small scales than the other members (Figure 8). This difference may be due to several factors. First, the grooves associated with Hvg and the ridges associated with Hvr can contribute to the small-scale roughness. Grooves are commonly linear and vertically distinctive in their topographic characteristics (several tens of meters [*Hiesinger and Head*, 2000]), as are the ridges associated with Hvr. The horizontal scale of these features is typically smaller than 3 km. Figure 9 shows an example of a MOLA profile taken from the Grooved Member, which illustrates that grooves are sharper features in comparison to the background Vastitas Borealis topography. It is seen also that grooves cut the background features in arbitrary places, not preferring either local lows or local highs. Although grooves and ridges actually occupy a small percentage of the surface, their linear aspect favors their sampling by MOLA profiles and allows them to contribute to the median differential slopes. A second factor for higher small-scale roughness of the Grooved Member may be the latitudinal trend (see section 4). A significant part of Hvg is situated in Utopia Planitia at relatively low latitudes, where the small-scale roughness is systematically higher.

The distinctive characteristics of the Vastitas Borealis Formation and its differences from virtually all other terrains suggest that its origin is different from other units on Mars. The outer margins of the Vastitas Borealis Formation correspond closely to the location of Contact 2 as mapped by *Parker et al.* [1989, 1993], who interpreted the contact to be an ancient shoreline of an ocean occupying the northern lowlands in middle Mars history. Tests using MOLA data have shown that several predictions are consistent with this hypothesis (e.g., altitude position of Contact 2, predicted sedimentation and smoothing below Contact 2, and implied volume of water) [*Head et al.*, 1999]. The close correlation of the Vastitas Borealis Formation boundaries with the position of Contact 2, the very smooth (in large scales) and homogeneous nature of the unit, and its location at the bottom of a drainage basin that comprises about two thirds of the planet [*Smith et al.*, 1999] are also consistent with the unit representing deposits from a standing body of water in middle Mars history. The detailed surface textures of the subunits (knobs, ridges, grooves, mottling) may have formed in response to modification processes associated with the loss of such a standing body of water or ice [e.g., *Kargel et al.*, 1995; *Head et al.*, 1999; *Hiesinger and Head*, 2000].

3.5. Volcanic Plains

Various volcanic plains units occupy a significant part of the Martian surface, forming most of the Tharsis region and appearing as larger or smaller patches amid cratered highlands. Figure 3 (curve Hr) shows the scale dependence of roughness for Lunae Planum (0°-20°N, 285°-305°E) as an example of Hesperian age volcanic plains [*Greeley and Guest*, 1987]. Lunae Planum is rougher than the Vastitas Borealis Formation at small and large scales and has similar roughness at the intermediate scales. These relatively low (in comparison to highlands) values of roughness with a prevalence of small-scale roughness produce cold gray shades in the map (Plate 1, boxes O4-O5). The roughness decreases linearly in the log-log plot, corresponding to a power law with an exponent of -0.27.

The topography of Lunae Planum is controlled by a set of different features of different scales: lava flow fronts (at small

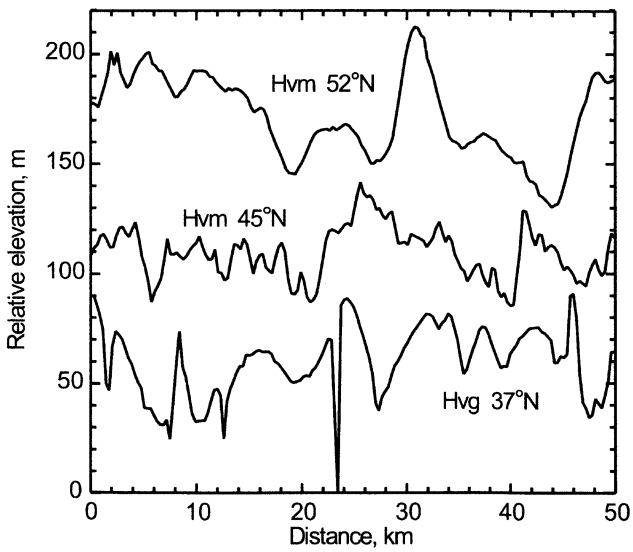

Figure 9. Examples of MOLA profiles from the Vastitas Borealis Formation: Hvm, 45°N, Utopia Planitia in "rough band," orbit 10090, 45°N, 89°E; Hvm, 52°N, Utopia Planitia to the north from "rough band," orbit 10090, 37°N, 90°E; Hvg, 37°N, grooved terrain in Utopia Planitia, orbit 10077, 37°N, 103°E. Profiles are arbitrarily shifted vertically. The vertical axis is considerably stretched in comparison to Figure 2.

scale), tectonic features, mostly wrinkle ridges (at intermediate and large scales), impact craters (at all scales), and minor traces of erosion and sedimentation. This area is a good example of the surface that displays perfect power law scale dependence of roughness but is not fractal.

The scale dependence of roughness for many other units mapped as volcanic plains is rather similar to that of Lunae Planum. Examples of such dependences are shown in Figure 10. There are some variations in roughness among volcanic plains. For example, the Syrtis Major Formation (Plate 1, D4-D5, Hs in Figure 10) is rougher (brighter in the map), while some units around Tharsis Montes (M4-M5 in Plate 1; At_4 and At_5 in Figure 10) are smoother (darker) than Lunae Planum (and even than Vastitas Borealis).

Most Hesperian age volcanic plains, e.g., Hesperia Planum (F6 in Plate 1), the Syrtis Major Formation (D4-D5), Lunae Planum (O4-O5), and Solis Planum (O6), are systematically rougher than most Amazonian age volcanic plains, e.g., the Tharsis Formation members (L6-N4) and the Plains Member of the Olympus Mons Formation (L4). In turn, Noachian plains (unit Npl_3 according to *Scott and Tanaka* [1986] and *Greeley and Guest* [1987]) are systematically rougher than Hesperian age volcanic plains at each scale. This age trend is explained, at least partly, by accumulation of impact craters and tectonic deformation features on older plains. For the Amazonian age volcanic plains shown in Figure 10 (members At_4 and At_5 of the Tharsis Formation, the Plains Member Aop of the Olympus Mons Formation) a similar trend is observed: younger units are smoother. However, such a trend is not universal.

Roughness of all volcanic plains decreases with increase of scale and often follows well a power law with the exponents -0.2 to -0.3, although some deviations from the power law are observed. Such deviations cause colored shades in the roughness map, for example, in Dedalia Planitia (Plate 1, L6-M6). However, the volcanic plains never show a dominance of intermediate-scale roughness as occurs for the Vastitas Borealis Formation.

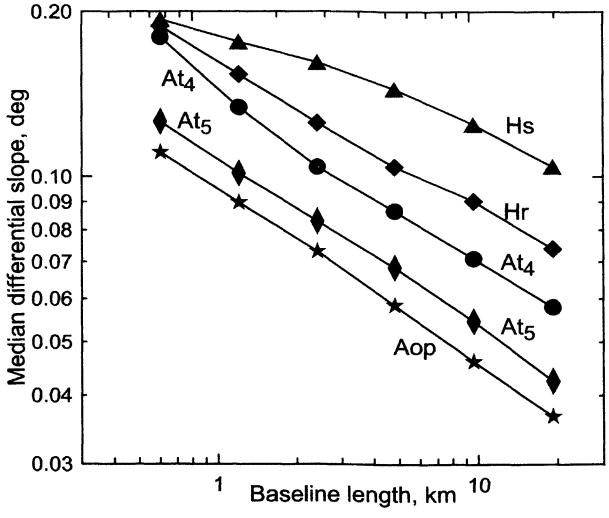

Figure 10. Dependence of the median differential slope on baseline length for selected volcanic plains units: Hs, Syrtis Major Formation; Hr, ridged plain in Lunae Planum; At_4, At_5, two major members of Tharsis Formation; Aop, Plains Member of Olympus Mons Formation. The vertical scale is the same as in Figure 8 and is considerably stretched in comparison to Figure 3.

3.6. Arcadia Formation

Amazonis Planitia is a very smooth region (profile Aa_3 in Figure 2). The median differential slope calculated over the Aa_3 member of the Arcadia Formation [*Scott and Tanaka*, 1986], which is the dominant geological unit in this region, is shown in Figure 3. The roughness decreases with increase of the baseline length (Aa_3 in Figure 3), but this decrease is less steep than that for the linear dunes in Olympia Planitia (Adl). The general smoothness means a dark shade in the roughness map, and the prevalence of small-scale roughness gives some intensity in the blue channel; the resulting shade on the map is dark blue (Plate 1, boxes J4 and K4).

Although Amazonis Planitia is a part of the northern lowlands, its roughness characteristics are very distinctive from the Vastitas Borealis Formation: Amazonis Planitia is much smoother at all scales and shows no dominant scale of topography. This suggests a different origin of the Arcadia Formation. The Arcadia Formation members in Arcadia Planitia (Plate 1, G3) are rougher than Amazonis Planitia and closer to Vastitas Borealis in roughness characteristics, though still distinctive.

The Arcadia Formation is interpreted as being composed of lava flows and to be of volcanic origin [*Scott and Tanaka*, 1986]. The general smoothness, absence of a characteristic scale of topography, and monotonic decrease of roughness with increase of scale make the roughness characteristics of the Arcadia Formation similar to those of other volcanic plains. However, the differences in roughness are also important: Amazonis Planitia is much smoother than other volcanic plains on Mars, and the decrease of roughness with increase of scale is steeper (compare Aa_3 and Hr in Figure 3); the power law exponent is –0.65 in contrast to -0.2 to -0.4 for other volcanic plains. These differences imply differences in the emplacement style of the Arcadia Formation relative to other volcanic plains.

The eastern part of Elysium Planitia has roughness characteristics very similar to Amazonis Planitia (dark blue in the map, Plate 1, box I5). Thus the very smooth and similar nature of eastern Elysium Planitia (Plate 1, I5), Amazonis Planitia (bottom of JK3, top of K4, and K4), and Marte Valles, which connects the two (lower left of J4), suggests that they are related. In agreement with this suggestion, the morphology of well-preserved flood lavas very similar to the morphology of Amazonis Planitia is seen in high-resolution MGS Mars Orbiter Camera (MOC) images of this region [*McEwen et al.*, 1999]. Eastern Elysium Planitia is the site of the Cerberus Formation, mapped by *Plescia* [1990] and interpreted to be very young flood lavas. MOC images show that these deposits are characterized by a distinctive surface texture that is different from the more lobate flow-front-dominated volcanic plains typical of other units interpreted to be volcanic in Tharsis and Elysium. On the basis of these characteristics, and differences from other units, *McEwen et al.* [1999] and *Keszthelyi et al.* [2000] interpreted this unit as very young flood basalts. The deposits have a very distinctive texture in MOC images, being dominated by broad plates and low ridges and by textures interpreted to represent rafted crustal slabs, ponded surfaces, possible squeeze ups, and a few rare channel-like features. The distinctive fine-scale texture seen in the MOC images is represented by radar-bright returns at radar wavelengths at the decimeter scale [e.g., *Harmon et al.*, 1992, 1999], below the resolution of the MOLA data. However, at longer scale lengths our data illustrate that the deposit is extremely smooth, consistent

with the interpretation that it is a young flood lava forming a very distinctive regionally smooth surface [e.g., *Hartmann et al.*, 1999; *McEwen et al.*, 1999; *Keszthelyi et al.*, 2000] and differing from the flow-lobe-dominated deposits of many other volcanic units.

3.7. Polar Deposits

The polar caps are clearly distinguished in the roughness maps (Plate 2) with their red or reddish color. A red color means a low intensity in the green and blue channels, which indicates that the polar caps are smooth at kilometer and subkilometer scale. An example of a MOLA profile taken from the north residual ice deposits (Api in Figure 2) demonstrates the absence of small-scale features in the profile and the presence of troughs of 10-km scale. The trough shown as an example in Figure 2 is relatively small; many troughs are much deeper and steeper. The increase of roughness at large scales (Api in Figure 3) reflects the presence of the troughs. The lower left corner of Figure 3 cut by the dashed line is the domain where MOLA ranging accuracy (reported by *Smith et al.* [1999] to be 0.3 m) is insufficient for precise estimation of the median differential slope. The increase of roughness at the shortest baseline (Api in Figure 3) is probably due to measurement noise rather than due to the presence of small-scale topographic features.

Unlike the plains units, the polar caps are not homogeneous in the roughness map (Plate 2): the surface between the troughs is perfectly smooth at all scales, while troughs are rougher, especially at large scales.

Figure 11 shows the scale dependences of roughness for different polar deposits (note that the vertical axis is stretched in comparison to Figure 3). South pole icy deposits (Api S, Figure 11) are much rougher than the same unit at the north pole (Api N), especially for shorter baselines. This indicates a difference in the deposition and sublimation regimes on the caps. Difference in surface morphology between the residual ice caps was observed also with the high-resolution MOC images [*Thomas et al.*, 2000]. The southern ice displays a number of 100-m-scale features, which are interpreted as being a result of sublimation of few-meter-thick CO_2 deposits by *Thomas et al.* [2000]. The northern polar cap is probably free from such deposits, and the surface displays only meter-scale roughness.

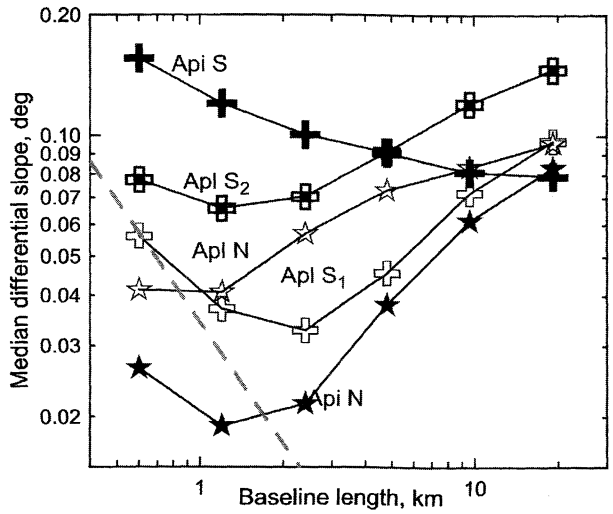

Figure 11. Dependence of the median differential slope on baseline length for the polar caps. Api N and Api S, residual ice deposits, the north and south caps, respectively; Apl N, layered terrains of the north cap; Apl S_1, layered terrains of the south cap in the 170°-240°E sector; Apl S_2, layered terrains of the rest of the south cap. The dashed line shows the limit of MOLA measurement accuracy. Logarithmic scale on both axes. The vertical scale is stretched in comparison to Figure 3.

Layered terrains near the north pole (Apl N) are systematically rougher than the icy surface (Api N) at shorter baselines. However, the median differential slope increases with the increase of the baseline length, indicating that kilometer-scale topography for the layered terrains is dominated by large-scale features as it is for the icy deposits. We subdivided the extended southern layered terrains into two subregions: the smooth plateau (Apl S_1) (170°-240°E) and the rest of the polar deposits (Apl S_2). Of course, Apl S_1 is smoother than Apl S_2 (Figure 11). Both subregions show a scale dependence of roughness similar to that for northern layered deposits.

Note that roughness at the longest baselines is similar for all polar units. This suggests that the mechanism of trough formation [e.g., *Howard et al.*, 1982; *Thomas et al.*, 1992], which is responsible for this topography (creep of ice-rich material and/or its sublimation), is the same for both polar caps and for both icy and layered deposits.

3.8. Medusae Fossae Formation

The Medusae Fossae Formation [*Scott and Tanaka*, 1986; *Greeley and Guest*, 1987] is superposed over the Martian dichotomy boundary in the form of several patches. These patches are clearly seen in the roughness map (Plate 1, H5-K5) thanks to their contrasting coloring. The surface of the formation is much rougher (brighter) than all northern lowlands and highland volcanic plains and noticeably smoother than the equatorial highlands. Despite the distinctiveness of its roughness signature from surrounding terrains, the Medusae Fossae Formation does not show a well-defined characteristic scale dependence of roughness. The color of this formation in the roughness map (Plate 1) varies from cyan (due to the dominance of its heavily eroded surface) to pink and orange (due to the dominance of its well-defined general high, long-scale-length topography) [e.g., *Sakimoto et al.*, 1999].

3.9. Dorsa Argentia Formation

The Dorsa Argentea Formation [*Tanaka and Scott*, 1987] consists of plains terrains around the south polar cap. They are hypothesized to form as a result of retreat of extended polar cap in the Hesperian [*Head*, 2000]. Roughness characteristics of the Dorsa Argentea Formation are rather similar to those of the Vastitas Borealis Formation (green shades in Plate 2). However, the Dorsa Argentea Formation is somewhat rougher, and the roughness maximum at 3-km baseline is less pronounced than those for the northern plains. The roughness characteristics of the southern plains are not as uniform as that of the northern plains. A part of the Dorsa Argentea Formation inside the Prometheus basin, including the Chasma Australe floor, differs in its roughness from the rest of the formation: it is noticeably rougher at small scales (bluish shades in Plate 2).

3.10. The Smoothest Site and MOLA Ranging Accuracy

If the surface were ideally flat, the elevation measured by MOLA would be scattered around the true elevation value due to measurement noise. White Gaussian noise is probably a good

stochastic model for this measurement noise. For this model, in (1) all four elevations h are independent Gaussian random variables with the same standard deviation σ. Then their linear combination given by (1) is also a Gaussian random variable with the standard deviation of $\sqrt{5/2}\sigma l^{-1}$. The median absolute value for the Gaussian distribution is 0.674 of its standard deviation. Thus, for an ideally flat surface we expect the following dependence of our roughness measure on the baseline length:

$$S(l) = 1.066\,\sigma\,l^{-1}, \quad (3)$$

where l is the baseline length and σ is the standard deviation of the measurement noise. If the surface is not ideally flat, but has only smooth large scale ($>>l$) topographical variations, the median differential slope will be the same.

We calculated the scale dependence of roughness for the smoothest part of the north polar cap, the area seen as an almost black patch in Plate 2a. This dependence is shown in Figure 3 (line S). The values of the median differential slope are below the accuracy boundary (dashed line) and show a perfect power law dependence on the baseline length, except the longest baselines. The power law exponent is less than -0.9, that is, rather close to -1 predicted by (3) for white noise. The frequency distribution of the differential slopes at all baselines in this area is close to a normal distribution. It is obvious that all small-scale roughness seen for this area is purely due to measurement noise. Using (3), we derived the amplitude (one standard deviation) of this noise. It turned out to be 20 cm. This gives us an independent estimate of the accuracy of MOLA ranging measurements. Of course, this is the accuracy for smooth and flat terrains; for steeper slopes, when the elevation variation within the MOLA footprint (~100 m in diameter [*Smith et al.*, 1999]) is significant, the accuracy is lower.

4. Latitudinal Trend of Roughness

4.1. Observations

4.1.1. Southern hemisphere. A latitudinal trend of roughness in the southern hemisphere of Mars is clearly seen in the roughness maps (Plates 1 and 2a). Warmer, orange shades dominate for rough (bright) terrains at high southern latitudes, while colder, bluish shades are more typical for the rough equatorial highland regions. The observed difference in the shades means that the high-latitude region has lower small-scale roughness in comparison to the equatorial zone. No prominent changes are seen at the longest baseline (red channel). The boundary of the smoothed terrains is diffuse and located at ~30°-50°S. Its latitudinal position seems to vary around the planet. Figure 12 shows a map of 0.6-km baseline roughness (the blue channel from the map in Plate 1) with a line that best represents the diffuse boundary.

To analyze the latitudinal dependence of roughness quantitatively, we chose highland areas belonging to the same geological unit, namely, unmodified highland plateau Npl_1, according to the geological maps [*Scott and Tanaka*, 1986; *Greeley and Guest*, 1987]. Then we calculated the median differential slopes for a number of narrow latitudinal zones within this unit. We did this separately for the 90°–270°E hemisphere (Terra Cimmeria and Terra Sirenum) and for the 270°–90° hemisphere (Noachis Terra). Figure 13 shows the latitudinal dependence of roughness calculated in this way. It is seen that the small-scale roughness displays ~3 times decrease at high south latitudes, although there is almost no latitudinal dependence for the large-scale roughness. The boundary is located at ~30°S in the Noachis hemisphere and at ~50°S in the Cimmeria/Sirenum hemisphere.

The scale dependences of roughness northward and southward from the smoothness boundary are compared in Figure 14 for cratered highlands. The similarity for long baselines and smoothing in the south for short baselines is clearly seen. Figure 2 shows examples of MOLA profiles for smoothed (Npl_1 S) and not smoothed (Npl_1 R) terrains from the same geological unit. Of course, we cannot be sure that the chosen profiles are representative examples of the difference in topographic pattern responsible for the observed roughness trend. However, the higher small-scale sinuosity of the profile taken from the equatorial region is obvious (Figure 2).

To assess the characteristic vertical scale corresponding to the observed approximately threefold difference in the small-scale roughness of highlands, we performed some modeling. We generated a random profile providing the scale dependence of roughness very similar to the upper curve in Figure 14. To do this, we used an algorithm for generating a self-affine random process, described, for example, by *Schroeder* [1991]. Then we applied two different smoothing procedures to this model topography. One of them was a linear low-pass filter. We chose the parameters of the filter so that the scale dependence of roughness of the filtered model topography would be similar to the lower curve in Figure 14. The RMS deviation of the filtered topography from the initial model turned out to be 0.6 m. The other smoothing procedure simulated filling of all local (one MOLA shot) depressions with sediments of some thickness. We obtained the scale dependence of roughness similar to the lower curve in Figure 14 for the modeled sediment thickness of 2.5 m. Of course, we do not believe that the topography is well described by a self-affine random process and that the unknown process responsible for the observed change in roughness works like the smoothing models we used. However, our modeling shows with certainty that the characteristic vertical scale related to the latitudinal trend in the southern hemisphere is of order of several meters.

4.1.2. Northern hemisphere. The latitudinal trend of roughness also takes place in the northern hemisphere (Plates 1 and 2a and Figure 12), though it is not as obvious as in the southern hemisphere. The high intrinsic roughness contrasts between different terrains (e.g., the global dichotomy boundary coinciding with the global roughness contrast) make it more difficult to see the presence or absence of the trend. The northern part of Arabia Terra (30°–40°N, 0°–60°E) appears to have warmer shades in the roughness map (Plate 1, A3–C3). However, this impression is partly due to the extremely high large-scale roughness in the fretted terrains of Deuteronilus Mensae (B3). A noticeable decrease in small-scale roughness does occur in the eastern part of the region (Plate 1, C3), but here it may be related to a geologic boundary rather than to the latitude-related changes.

Clear diffuse boundaries of small-scale smoothness are seen in Chryse Planitia (Plate 1, boxes Q3-R3; Figure 12) and Utopia Planitia (D3-G3) at ~47°N, where this parallel crosses geologically homogeneous plains. Figure 9 shows examples of profiles taken from the Vastitas Borealis Formation (the Mottled Member) in Utopia Planitia on both sides of the boundary. The profile from 45°N is more sinuous in small scale than the profile from 52°N. It appears that in Utopia Planitia and possibly in Chryse Planitia there is a band of increased small-scale roughness at 35° -47°N latitude.

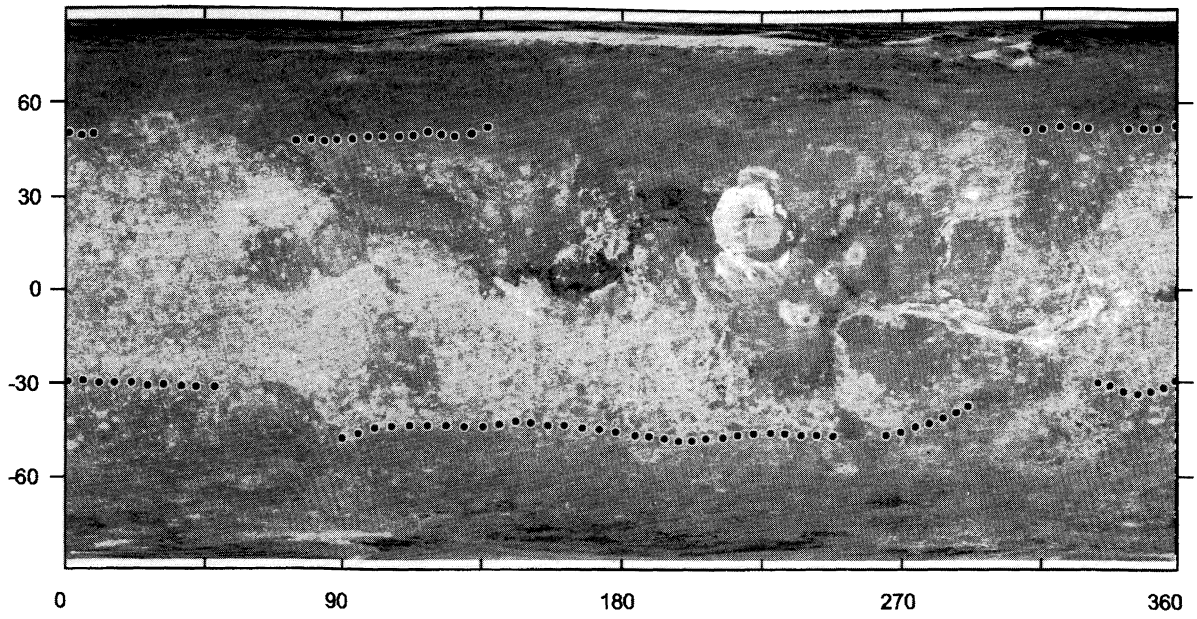

Figure 12. Map of the median differential slope at 0.6-km baseline. This map is the blue color separate from Plate 1. Map projection is simple cylindrical. Brighter shades denote rougher surface. Dots show approximate position of the diffuse boundary of the smoothed terrains.

The relative decrease in small-scale roughness at ~47°N is ~2-3 times, similar to the southern hemisphere. However, the corresponding vertical scale is somewhat smaller than in the southern hemisphere because of general smoothness of the northern plains.

4.1.3. Possible observation effects. MOLA operations and our data processing are not likely to introduce any latitude-dependent biases. Deviation of the Mars Global Surveyor orbit from a perfect circle is small. This deviation leads to systematic latitude-dependent variation in the shot-to-shot distance and hence the baseline length, but this variation does not exceed 5% and cannot account for the observed factor-of-3 difference in the small-scale surface roughness.

MGS passes are oriented close to the meridianal direction in an equatorial zone and make a larger angle to the meridian at higher latitudes. This can be a potential source of severe biases in the profile-derived roughness if the surface topography is strongly anisotropic. Such anisotropy occurs, for example, for fields of linear dunes (as in Figure 6) or sets of subparallel linear tectonic features. However, high-resolution Viking images did not reveal strong surface anisotropy either for cratered highlands in the southern hemisphere or for the Vastitas Borealis Formation in the northern hemisphere, where we observe the latitudinal trend. Thus we believe that the observed latitudinal trend indeed reflects changes in small-scale surface roughness.

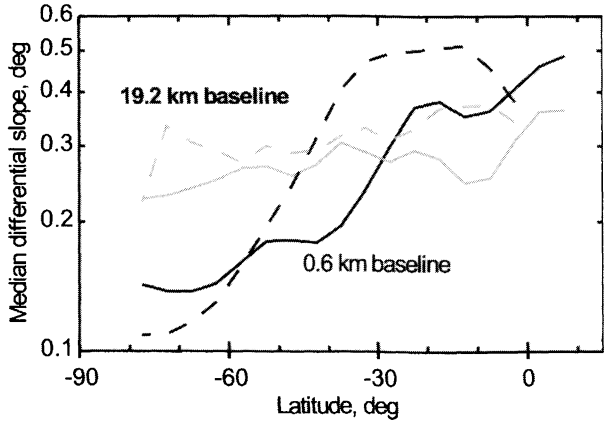

Figure 13. Latitudinal dependence of roughness in the southern hemisphere for the cratered highland plateau unit Npl_1: solid lines, longitudes from -90°E to 90°E (Noachis hemisphere); dashed lines, longitudes from 90° to 270°E (Cimmeria/Sirenia hemisphere); black lines, 0.6-km baseline; gray lines, 19.2-km baseline. Logarithmic scale on the vertical axis.

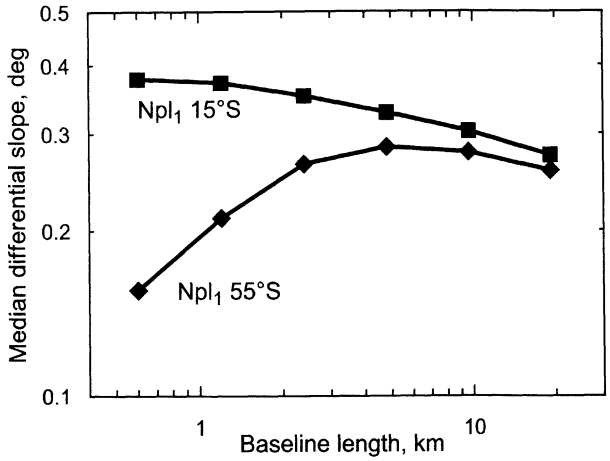

Figure 14. Dependence of the median differential slope on the baseline length for cratered highland plateau unit Npl1 in the Noachis hemisphere (-90°E to 90°E): upper curve, 5°-25°S zone; lower curve, 45° -65°S zone. Logarithmic scale on both axes. The vertical scale is considerably stretched in comparison to Figure 3.

MOLA data used in this study were obtained during Martian winter in the southern hemisphere, when the high-latitude zone approximately coinciding with the zone of observed smoothing was covered with seasonal CO_2 frost. We estimated the effect of converting the whole Martian atmosphere into frost and depositing it in local topographic lows and found that this cannot produce the observed smoothing. We used some MOLA data obtained later in the mission to test for seasonal variations in roughness. We found no evident changes. Seasonal roughness variations, if they exist in these data, are at least an order of magnitude weaker than the observed latitudinal smoothing. The observed latitudinal trend of roughness definitely survived the southern spring.

4.2. Relation to Other Data

Below, we review some observations showing any latitudinal trends and discuss how these observations can be related to the roughness trend observed.

4.2.1. Terrain softening. Terrain softening discovered by *Squyres and Carr* [1986] in high-resolution Viking images is the only morphological observation directly related to the latitudinal trend of roughness. The definitive morphological feature of softened terrains is that impact craters appear to have broader, more gently rounded rims [*Squyres and Carr*, 1986]. Such peculiarities of crater morphology are not reflected in the roughness maps, because the median values are not sensitive to rare specific features like crater walls, but reflect the most typical surface topography pattern. Between large craters, softened terrains are usually smoother and lack sharp surface details like small ridges [*Squyres and Carr*, 1986]. The absence of small sharp details in 50-100 m-per-pixel-resolution Viking images means decreased roughness at ~ 1 km scale and should be noticeable in the roughness maps.

Squyres and Carr [1986] mapped the distribution of softened terrains for the entire surface covered with high-resolution Viking images. (Their map is reproduced in [*Squyres et al.*, 1992].) They found no terrain softening in the equatorial zone of the planet up to 25°N and 25°S, though the high-resolution image coverage of this zone is good. In high southern latitudes, there is little data on Terra Sirenium and Terra Cimmeria (G-I 7-8 in Plate 1). *Squyres and Carr* [1986] found terrain softening in Noachis Terra, Hellas Planitia, and Promethei Terra (B-F 7-8, Plate 1). Almost all of the area of high-resolution coverage south of 40°S displays terrain softening. From the mapping of *Squyres and Carr* [1986] it appears that the boundary of the softened terrains is located at ~25°S in Noachis Terra (A-B7) and at ~40°S in Terra Cimmeria (G-I7). Thus the longitudinal difference of the boundary position of softened terrains correlates with that for the smoothed terrains (see above).

The northern hemisphere is better covered with high-resolution Viking images. The *Squyres and Carr* [1986] survey showed that softened terrains in the northern hemisphere do not form a continuous band. Softening is observed in the northern part of Arabia Terra (A-C 3, Plate 1), Acheron Fossae (L3), and Tempe Terra (O3). In Arabia Terra and Tempe Terra the southern boundaries of the softened regions are at ~25°N.

Thus we see some correlation between the spatial distribution of smoothed and softened terrains, including longitudinal variations of the boundary in the southern hemisphere. However, the spatial distribution of the softening and smoothing do not coincide. Some softened terrains in the northern hemisphere, including the best examples considered by *Jankowski and Squyres* [1992], do not show apparent smoothing in the roughness map, or smoothing is doubtful, while the vast smooth part of the northern plains is not softened.

In summary, the morphologically observed terrain softening may contribute to the latitudinal trend of roughness, but it does not account for the whole effect.

4.2.2. Small-scale surface texture. The observed latitudinal dependence of smoothing is most pronounced at small scale, <1 km. This means that the surface features related to smoothing can be seen only in images with high (better than 100 m) resolution. However, the high variability of small-scale surface texture on Mars inhibits morphological observations related to the trend. High-resolution Viking coverage of the high southern latitudes, where the trend is best presented, is poor.

We performed a systematic survey of all high-resolution MOC images [*Malin et al.*, 1998] in a few-degree-wide band around the smoothing boundary at 47°N in western Utopia Planitia (Plate 1, upper 1/3 of box 3E), where this boundary goes across a typical Vastitas Borealis Formation surface. All images released so far were used in the survey (images obtained through August 1999), a total of 40 images. We found well-expressed difference between a background surface texture on both sides of the boundary. The rough domain southward from 47°N has an impressive pattern of 100-m to 1-km-scale steep pits and scarps (Figure 15a, upper left and lower parts of Figure 15c). Northward from 47°N the surface lacks apparent tens-of-meters-scale topographic features and is dominated by fine homogeneous regular hummocky texture with well-defined characteristic texture size, which varies from image to image from several meters (Figure 15b) to almost unresolved (Figure 15c, center). A few images on the diffuse boundary of the smooth and rough domains show that the smooth fine-textured material possibly overlays pits and scarps characteristic of the rough domain (Figure 15c); however, the images available so far do not allow us to establish this relationship with complete confidence.

In other regions the surface texture in the high-resolution MOC images displays much higher variability, and the systematic differences responsible for the roughness trend are not as clearly identified as in western Utopia Planitia. Our selective examination of surface texture in the northern lowlands showed that the variants of the smooth fine-textured pattern are typical in the northern part of Vastitas Borealis. Images on both sides of the smoothing boundary in southern highlands, in Terra Cimmeria, show rough topography north of the boundary (Figure 15d) and smooth terrain south of the boundary (Figure 15e). The surface pattern in the image taken from the smooth domain (Figure 15e) is similar to that observed in the smooth domain in Utopia Planitia (Figure 15b). Additional study of larger numbers of images is necessary to assess how typical these differences are.

4.2.3. Other morphological observations. Distribution of valley networks on Mars displays a prominent latitudinal trend: valleys are concentrated in the 65°N-65°S belt, and decrease in number toward the high latitudes [e.g., *Baker et al.*, 1992]. Valleys have widths from <1 km to nearly 10 km and often have short steep slopes [e.g., *Baker et al.*, 1992]. Their linear aspect favors sampling with MOLA profiles. This means that valley networks contribute to increased roughness of equatorial terrains in comparison to polar areas. However, this contribution is not likely to be important for the following reasons. First, the total area covered by valleys is small. Second, valleys are observed mostly in cratered terrains, while

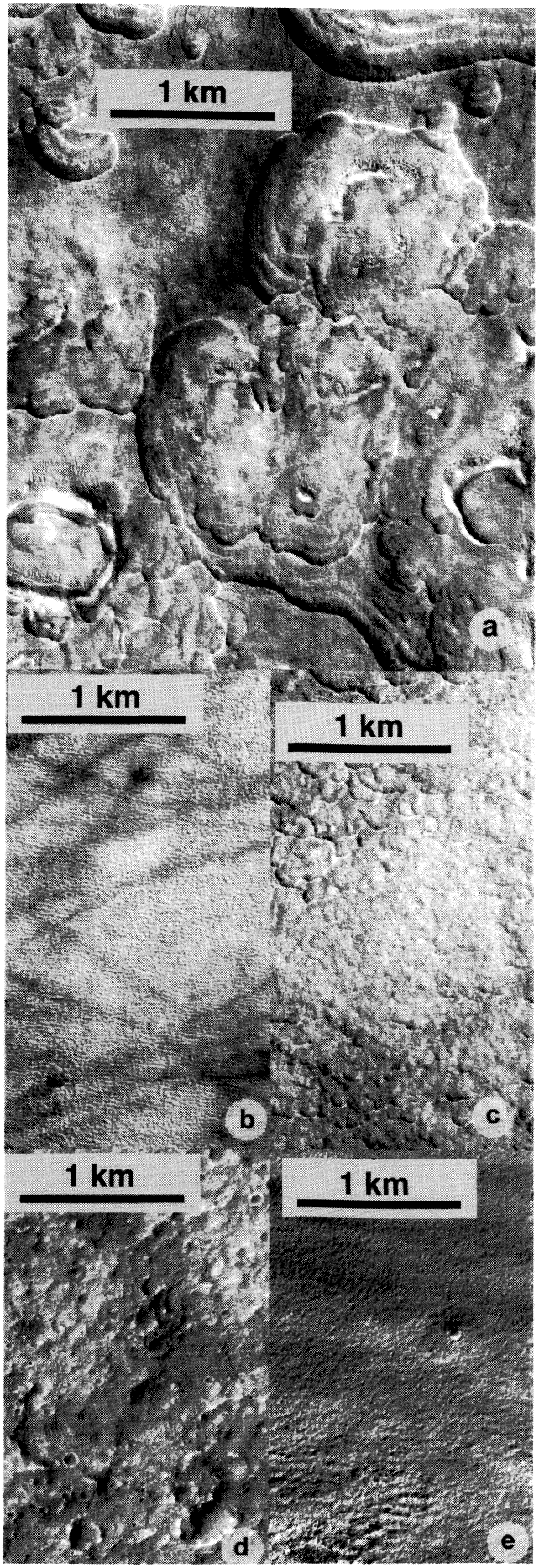

the rough equatorial band consists of various types of terrains, including old plains units bearing no valleys. Third, valleys appear on the Martian surface in clusters, but there is no obvious correlation between the location of valley networks mapped by *Mars Channel Working Group* [1983] and small-scale roughness. Finally, valleys cannot be related to the latitudinal roughness boundaries in the northern lowlands.

Soderblom et al. [1973] surveyed the present debris distribution in Mariner 9 high-resolution images. They showed that the present distribution of debris is strongly correlated with latitude and is symmetrically distributed around both polar regions, extending poleward from 30°N and 30°S latitudes. The survey was based on the apparent depth of the impact craters. Hence these observations deal with larger spatial scale than the observed roughness trend. *Soderblom et al.* [1973] interpreted the mantles observed to represent eolian debris derived from circumpolar layered deposits and redistributed equatorward by wind action.

Mustard and Cooper [2000] recognized a very specific pattern of small-scale steep topography using high-resolution MOC images. They interpreted this pattern as dissected duricrust. This pattern is observed only in 30°-60°N and 30°-60°S latitudinal zones with concentration toward the centers of these zones and through all longitudes. Although the characteristic spatial scale of topographic variations in these features is much smaller than the MOLA shot-to-shot distance, this irregular topography could contribute to the kilometer- and subkilometer-scale roughness.

4.2.4. Surface properties. The northern part of Mars (northward from ~20°S) shows high-amplitude regional-scale variations of thermal inertia and albedo, which anticorrelate with each other and show little correlation with surface morphology and latitude [e.g., *Christensen and Moore*, 1992]. Some specific relatively recent surface deposits probably completely removed all traces of geological history in albedo and thermal inertia patterns in this part of the planet [e.g., *Christensen and Moore*, 1992]. Southward from ~20°S the variations of albedo and thermal inertia are of smaller amplitude, have a smaller scale of spatial pattern, and show some correlation with morphological features.

Figure 15. (a) High-resolution image showing the typical surface in western Utopia Planitia southward from the smoothing boundary. Fragment of MOC narrow-angle camera image M04/02077. The scene is centered at 45.7°N, 91.5°E. (b) High-resolution image showing the typical surface in western Utopia Planitia northward from the smoothing boundary. Fragment of MOC narrow-angle camera image M03/02115. The scene is centered at 51.4°N, 92.4°E. (c) High-resolution image showing possible transition from not smoothed to smoothed terrain in western Utopia Planitia. Fragment of MOC narrow-angle camera image M03/04333. The scene is centered at 57.6°N, 86.6°E. (d) High-resolution image showing a terrain in Terra Cimmeria northward from the smoothing boundary. Fragment of MOC narrow-angle camera image M04/02033. The scene is centered at 31.9°S, 130.9°E. (e) High-resolution image showing a terrain in Terra Cimmeria southward from the smoothing boundary. Fragment of MOC narrow-angle camera image M04/04140. The scene is centered at 50.5°S, 127.2°E. In all images, north is approximately at the top. Image resolution is ~2.8 m per pixel. In Figures 15a-15c, illumination is from the southwest; in Figures 15d and 15e, illumination is from the northwest. Brightness and contrast adjustments are different for all images.

Albedo at 20°-40°S is generally lower than at higher southern latitudes. This trend is unambiguous; however, it is not as pronounced as the trend in subkilometer-scale roughness. Some systematic decrease of thermal inertia at high southern latitudes also can be noted. The lower values of thermal inertia are interpreted to mean the presence of a fine-grained surface layer. In Terra Cimmeria at ~40°S there is a rather sharp latitudinally oriented boundary in the thermal inertia map derived from the Viking observations [e.g., *Christensen and Moore*, 1992]; thermal inertia is lower southward from this boundary. In this region the latitudinal boundary in our roughness map is the sharpest (Plate 1, F7-I7) and coincides with the thermal inertia boundary rather well. The thermal inertia map derived from recent MGS observations [*Jakosky et al.*, 2000] also shows this boundary, although it is not so well expressed as in the older map. Probably, the change of subkilometer-scale roughness and thermal inertia with latitude in this region are related genetically, while in other regions the thermal inertia is influenced by some different surface processes.

Note that the thermal inertia is defined by properties of an upper layer ~10 cm thick, while albedo is controlled by a several-millimeter-thick layer. Hence these surface properties may not reflect the observed smoothing, whose characteristic vertical scale is of the order of several meters.

4.2.5. MOLA pulse-width roughness. *Garvin and Frawley* [2000] reported preliminary results of mapping of roughness derived from the pulse-width MOLA measurements. This roughness is a characteristic vertical scale of topography within a single 100-m-size MOLA footprint. Thus the spatial scale of this roughness is almost an order of magnitude shorter than the small scale in the present study. The vertical roughness derived from the pulse-width measurements shows strong variations often not related to geological boundaries. In particular, a high-latitude part of the northern plains is much smoother than the low-latitude part. Detailed comparison of the kilometer-scale roughness and the pulse-width roughness will be possible when the pulse-width mapping is accomplished.

4.3. Possible Origin

The observed latitudinal trend of roughness can be produced by a latitude-dependent process, which either makes the surface at low latitudes rougher or makes the surface at high latitudes smoother. Below, we overview several possible climate-dependent processes and evaluate them as candidates for the observed trend.

4.3.1. Creep of ice-rich material. Terrain softening was attributed to creep of an upper layer of ice-rich regolith [*Squyres and Carr*, 1986]. Several morphological observations indicate that such creep indeed occurred in the walls of some impact craters [*Squyres and Carr*, 1986; *Squyres et al.*, 1992]. A number of independent observations provide evidence for the presence of near-surface ground ice everywhere at high latitudes [e.g., *Squyres et al.*, 1992]. Hence creep of a near-surface ice-rich layer could contribute to the observed latitudinal trend of roughness. The creep could be more effective during hypothesized periods of higher obliquity of the planet; during these periods the climate is thought to be warmer [e.g., *Ward*, 1992].

However, creep alone is not a complete explanation for the observed trend of roughness. *Jankowski and Squyres* [1992] found that craters of 2-10 km in diameter in softened terrains are systematically much shallower than craters of the same size in terrains not softened. Creep able to produce such differences, if it operates over the whole surface rather then at the steepest slopes, would reduce 5-km-scale roughness at least as strongly as 0.6-km-scale roughness, which is not observed. In Utopia Planitia the southern boundary of the near-surface ice, obtained from peculiarities of impact crater morphology, is located at ~30°N [*Squyres et al.*, 1992]. The roughness map (Plate 1, D3, E3) shows an increase in the small-scale roughness northward from this boundary, while smoothing begins far northward, at ~47°N. Our observations of small-scale surface texture in this region (section 4.2.2) also do not favor creep as a process responsible for smoothing.

4.3.2. Seasonal polar cap. The observed smoothing zones approximately coincide with the extent of the seasonal frost [e.g., *James et al.*, 1992] in both hemispheres. The extent of the seasonal frost is expected to vary with geologically fast precession and obliquity oscillations. The characteristic timescale of these oscillations is of the order of 10^5 years [e.g., *Ward*, 1992]. We cannot exclude the possibility that the smoothing boundary is genetically related to the present seasonal frost boundary and follows its response to obliquity- and precession-induced climate variations. However, such flexibility of surface topography at ~1-m vertical scale is hardly compatible with the preservation of <100-m vertical scale features on Mars during billions years. It is more probable that the observed position of the smoothing boundary reflects some effect averaged over climate variations and the coincidence with the present seasonal caps is occasional rather than genetic. This agrees with the present obliquity being in the middle of the limits of its variations [e.g., *Ward*, 1992].

Nevertheless, the seasonal frost might contribute to formation of the latitudinal trend of roughness. Deposition and sublimation of the seasonal frost may operate on geological timescales as a gentle eroding factor, favoring downslope movement of eroded material and hence smoothing of topography at small scales. This mechanism also could be more effective during periods of higher obliquity with more intensive seasonal changes and wetter climate [e.g., *Ward*, 1992]. During such periods, inclusion of H_2O into seasonal frost deposits could increase the effect of erosion. We do not see morphological evidence for enhanced downslope movement in the high-resolution images. Thus we believe that this mechanism is not probable.

The seasonal frost also could play a role in formation of smoothing mantles as an agent favoring deposition of fine dust and/or cementation of the deposited dust. Dust particles can serve as seeds for H_2O and CO_2 crystals growing in the atmosphere during winter. This gathers the dust in the atmosphere and delivers it to the surface, contributing to net dust deposition in the regions of the seasonal caps. Small amounts of H_2O inevitably present in the seasonal cap [e.g., *Jakosky and Haberle*, 1992] could cause chemical reactions that lead to cementation of the dust deposits, which prevents removal of the deposited dust by winds. Cementation can be much more effective during epochs of higher atmospheric pressure, when the H_2O content was higher and minor amounts of H_2O could be in a liquid phase during the recession of the seasonal frost.

4.3.3. Atmospheric circulation. Deposition of smoothing mantles at high latitudes could also occur because of wind-forced dust migration. In the present epoch the redistribution of the fine dust observable as changes of surface albedo features does not have any pronounced zonal pattern [e.g., *Kahn et al.*, 1992]. Redistribution of sand modeled by *Anderson et al.* [1999] also does not resemble the roughness trend. However, climate changes inevitably lead to changes of the atmospheric circulation pattern. Dust migration balanced over

a number of obliquity cycles might lead to net dust removal at low latitudes and deposition at high latitudes.

Wind-controlled dust migration could be accompanied with trapping of the dust with processes of cementation. These processes could be controlled by climate- and hence latitude-dependent factors, e.g., temperature and humidity, as well as the seasonal frost mentioned above.

4.3.4. Sublimation and accumulation of near-surface ice. Modeling by *Mellon and Jakosky* [1995] showed that the obliquity variations produce cyclic saturation of the top 1 to 2 m of the regolith with ice and subsequent dessication. This occurs at low latitudes, while at high latitudes the ice is stable with respect to obliquity variations. This process can work as eroding agent, increasing the small-scale roughness in the equatorial zone, either directly forming specific small-scale features or indirectly eroding away smooth surficial mantles. Periodic sublimation of the subsurface ice can also provide a supply of dust for redistribution by winds.

The near-surface ice persisting in the high-latitude regions can favor cementation of the surface dust deposits through the presence of water vapor in the near-surface layer. In this way, the subsurface ice can provide a trap for dust redistributed by winds.

4.3.5. Discussion. Among numerous possible mechanisms of formation of the latitudinal trend considered above, we prefer those related to deposition of smooth several-meter-thick blankets in high-latitude areas. This preference is based on the apparent presence of such blankets in high-resolution images in western Utopia Planitia (Figure 15c; see section 4.2.2), where the smooth material appears to be deposited over a rougher surface. A lower thermal inertia seen in some smoothed regions in the southern hemisphere (section 4.2.4) is consistent with this hypothesis. Dissected duricrust observed by *Mustard and Cooper* [2000] (section 4.2.3) could represent the margins of such blankets.

Such deposits are of a vertical scale between that of geological features and of the uppermost surface layer. The surface layer is affected by season progression and weather-related processes (such as global dust storms). The timescale of these processes is of the order of a year, and the vertical scale affected by these processes does not exceed several centimeters. Changes at this timescale are observed in terms of surface albedo variations (uppermost layer) and thermal inertia (a few centimeters). Both of these scales are below that of the observed smoothing trend (several meters). Surface features starting from the vertical scale of tens of meters (e.g., the characteristic background topography of the Vastitas Borealis Formation) have persisted for geological timescales. The blankets responsible for the latitudinal trend of roughness are of the order of several meters thick. Probably, the characteristic time of their formation comprises a number of climate change cycles but is much shorter than the longer geological timescales.

Further studies of topography and images are necessary to test our hypothesis smoothing mantles as a cause of the observed roughness trend. Such studies should clarify the roles of seasonal frost, subsurface ice dynamics, temperature and humidity conditions, and global wind pattern in formation of the mantles.

5. Conclusions and Future Work

We show that kilometer-scale surface roughness derived from statistical analysis of MOLA data can be a useful tool for interpretation of the properties of the Martian surface and the origin and evolution of geologic units. Below is a brief list of the results obtained in this paper.

1. The accuracy of MOLA range measurements for smooth surfaces is 20 cm (one standard deviation). This is an independent estimate obtained from the data themselves (section 3.8).

2. The southern polar cap is rougher than the northern at small (kilometer) scale, which suggests differences in the sublimation/condensation balance responsible for topography at this scale (section 3.7).

3. The Vastitas Borealis Formation has a distinctive 3-km-scale background surface topography, which suggests a non-volcanic origin for its upper layer (section 3.4).

4. Amazonis Planitia and the eastern part of Elysium Planitia have very similar roughness characteristics distinctive from other terrains on Mars, which suggests a similarity of their origin. The distinctive roughness characteristics suggest a distinctive flood-basalt eruption style, different than the lobate flows typical of Tharsis (section 3.6).

5. There are systematic latitudinal variations of kilometer-scale roughness, which suggests the presence of a debris mantle of several meters thickness and some climate-driven process of surface modification at these scales (section 4).

These findings show that analysis of kilometer-scale roughness and its scale dependence can be useful in the study of Mars. Processing of the entire set of MOLA data obtained later in the mission will allow us to obtain roughness maps of higher resolution and to study the scale dependence of roughness for smaller isolated areas, which will allow application of these data to local analysis of geology and processes.

In addition to a general measure of roughness, statistical analysis of MOLA profiles can provide general, more detailed characteristics of small-scale topographic patterns not seen in the digital elevation models.

Acknowledgments. We gratefully acknowledge the MOLA instrument team and MGS spacecraft and operation teams at the Jet Propulsion Laboratory and Lockheed-Martin Astronautics for providing the engineering foundation that enabled this analysis. We also acknowledge the use of Mars Orbiter Camera images processed by Malin Space Science Systems that are available at http://www.msss.com/moc_gallery/. This effort was supported by MOLA (NASA Mars Global Surveyor Project) and the Mars Data Analysis Program, NASA grant NAG5-8283. Thanks are extended to Greg Neumann and Steve Pratt for data management and very fruitful discussions on interpretation.

References

Aharonson, O., M. T. Zuber, G. A. Neumann, and J. W. Head, Mars: Northern hemisphere slopes and slope distributions, *Geophys. Res. Lett.*, *25*, 4413–4416, 1998.

Aharonson, O., M. T. Zuber, and G. A. Neumann, Second order statistics of topography of the northern hemisphere of Mars from MOLA, *Lunar Planet. Sci., XXX*, abstract 1792, 1999.

Albee, A. L., F. D. Palluconi, and R. E. Arvidson, Mars Global Surveyor Mission: Overview and status, *Science*, *279*, 1671-1672, 1998.

Anderson, F. S., R. Greeley, P. Xu, E. Lo, D. G. Blumberg, R. M. Haberle, and J. R. Murphy, Assessing the Martian surface distribution of aeolian sand using a Mars general circulation model, *J. Geophys. Res.*, *104*, 18,991-19,002, 1999.

Baker, V. R., M. H. Carr, V. C. Gulick, C. R. Williams, and M. S. Marley, Channels and Valley Networks, in *Mars*, edited by H. H. Kieffer, et al., pp. 493–522, Univ. of Ariz. Press, Tucson, 1992.

Christensen, P. R., and H. J. Moore, The Martian surface layer, in *Mars*, edited by H. H. Kieffer, et al., pp. 686-729, Univ. of Ariz. Press, Tucson, 1992.

Francis, P. W., and G. Wadge, The Olympus Mons aureole: Formation by gravitational spreading, *J. Geophys. Res.*, *88*, 8333-8344, 1983.

Garneau, S., and J. J. Plaut, Topographic and roughness characteristics of the Vastitas Borealis Formation on Mars described by fractal statistics, *Lunar Planet. Sci., XXXI*, abstract 1115, 2000.

Garvin, J. B., and J. J. Frawley, Global vertical roughness of Mars from Mars Orbiter Laser Altimeter pulse-width measurements, *Lunar Planet. Sci., XXXI*, abstract 1884, 2000.

Greeley, R., and J. E. Guest, Geological map of the eastern equatorial region of Mars, *U.S. Geol. Surv. Misc. Invest. Ser. Map I-1802-B*, 1987.

Greeley, R., N. Lancaster, S. Lee, and P. Thomas, Martian aeolian processes, sediments, and features, in *Mars*, edited by H. H. Kieffer, et al., pp. 730–766, Univ. of Ariz. Press, Tucson, 1992.

Harmon, J. K., M. P. Sulzer, P. J. Perillat, and J. F. Chandler, Mars radarmapping: Strong backscatter from the Elysium Basin and outflow channel, *Icarus*, *95*, 153-156, 1992.

Harmon, J. K., R. E. Arvidson, E. A. Guiness, B. A. Campbell, and M. A. Slade, Mars mapping with delay-Doppler radar, *J. Geophys. Res.*, *104*, 14,065-14,089, 1999.

Hartmann, W. K., M. Malin, A. S. McEwen, M. Carr, L. Soderblom, P. Thomas, E. Danielson, P. James, and J. Veverka, Evidence for recent volcanism on Mars from crater counts, *Nature*, *397*, 586-589, 1999.

Head, J. W., Extensive south polar ice cap in the middle Mars history?: Tests using MOLA data, *Lunar Planet. Sci., XXXI*, abstract 1119, 2000.

Head, J. W., and M. A. Kreslavsky, Mars northern lowlands: Topographic characteristics of members of the Vastitas Borealis Formation, *Lunar Planet. Sci., XXXI*, abstract 1279, 2000.

Head, J. W., H. Heisinger, M. A. Ivanov, M. A. Kreslavsky, S. Pratt, and B. J. Thompson, Possible ancient oceans on Mars: Evidence from Mars Orbiter Laser Altimeter data, *Science*, *286*, 2134-2137, 1999.

Hiesinger, H., and J. W. Head, Characteristics and origin of polygonal terrain in southern Utopia Planitia, Mars: Results from Mars Orbiter Laser Altimeter and Mars Orbiter Camera data, *J. Geophys. Res.*, *105*, 11,999-12,022, 2000.

Howard, A. D., J. A. Cutts, and K. R. Blasius, Stratigraphic relationships within Martian polar cap deposits, *Icarus*, *50*, 161-512, 1982.

Jakosky, B. M., and R. M. Haberle, The seasonal behavior of water on Mars, in *Mars*, edited by H. H. Kieffer, et al., pp. 969–1016, Univ. of Ariz. Press, Tucson, 1992.

Jakosky, B. M., M. T. Mellon, H. H. Kieffer, P. R. Christensen, E. S. Varnes, and S. W. Lee, The thermal inertia of Mars from the Mars Global Surveyor Thermal Emission Spectrometer, *J. Geophys. Res.*, *105*, 9643-1652, 2000.

James, P. B., H. H. Kieffer, and D. A. Paige, The seasonal cycle of carbon dioxide on Mars, in *Mars*, edited by H. H. Kieffer, et al., pp. 934–968, Univ. of Ariz. Press, Tucson, 1992.

Jankowski, D. G., and S. W. Squyres, The topography of impact craters in "softened" terrains on Mars, *Icarus*, *100*, 26-39, 1992.

Kahn, R. A., T. Z. Martin, R. W. Zurek, and S. W. Lee, The martian dust cycle, in *Mars*, edited by H. H. Kieffer, et al., pp. 1017–1053, Univ. of Ariz. Press, Tucson, 1992.

Kargel, J. S., V. R. Baker, J. E. Beget, J. F. Lockwood, T. L. Pewe, J. S. Shaw, and R. G. Strom, Evidence of continental glaciation in the Martian northern plains, *J. Geophys. Res.*, *100*, 5351-5368, 1995.

Keszthelyi, L., A. S. McEwen, and T. Thordarson, Terrestrial analogs and thermal models for Martian flood lavas, *J. Geophys. Res., 105*, 15,027-15,049, 2000.

Kreslavsky, M. A., and J. W. Head, Kilometer-scale slopes on Mars and their correlation with geologic units: Initial results from Mars Orbiter Laser Altimeter (MOLA) data, *J. Geophys. Res.*, *104*, 21,911-21,924, 1999.

Kreslavsky, M. A., and J. W. Head, Kilometer-scale roughness of Martian surface from MOLA data: Characterization of geological units, *Lunar Planet. Sci., XXXI*, abstract 1144, 2000a.

Kreslavsky, M. A., and J. W. Head, Kilometer-scale roughness of Martian surface from MOLA data: A latitudinal trend, *Lunar Planet. Sci., XXXI*, abstract 1145, 2000b.

Malamud, B. D., and D. L. Turcotte, Wavelet analysis of Mars MOLA topography, *Lunar Planet. Sci., XXXI*, abstract 1016, 2000.

Malin, M. C., et al., Early views of Martian surface from the Mars Orbiter Camera of Mars Global Surveyor, *Science, 279*, 1681-1685, 1998.

Mars Channel Working Group, Channels and valleys on Mars, *Geol. Soc. Am. Bull.*, *94*, 1035-1054, 1983.

McEwen, A., M. Malin, L. Keszthelyi, P. Lanagan, R. Beyer, and W. Hartmann, Recent and ancient lavas on Mars, *Lunar Planet. Sci., XXX*, abstract 1829, 1999.

Mellon, M. T., and B. M. Jakosky, The distribution and behavior of Martian ground ice during past and present epochs, *J. Geophys. Res., 100*, 11,781-11,799, 1995.

Mustard, J. F., and C. D. Cooper, Global distribution of dissected duricrust on Mars, *Lunar Planet. Sci., XXXI*, abstract 1168, 2000.

Parker, T. J., R. S. Saunders, and D. M. Schneeberger, Transitional morphology in West Deuteronilus Mensae, Mars: Implications for modification of the lowland/highland boundary, *Icarus*, *82*, 111-145, 1989.

Parker, T. J., D. S. Gorsline, R. S. Saunders, D. C. Pieri, and D. M. Schneeberger, Coastal geomorphology of the Martian northern plains, *J. Geophys. Res.*, *98*, 11,061-11,078, 1993.

Plescia, J. B., Recent flood lavas in the Elysium region of Mars, *Icarus*, *88*, 465-490, 1990.

Sakimoto, S. E. H., H. V. Frey, J. B. Garvin, and J. H. Roak, Topography, roughness, layering, and slope properties of the Medusae Fossae Formation from Mars Orbiter Laser Altimeter (MOLA) and Mars Orbiter Camera (MOC) data, *J. Geophys. Res.*, *104*, 24,141-24,154, 1999.

Schroeder, M., *Fractals, Chaos, Power Laws: Minutes From an Infinite Paradise*, W. H. Freeman, New York, 1991.

Scott, D. H., and K. L. Tanaka, Geological map of the western equatorial region of Mars, *U. S. Geol. Surv. Misc. Invest. Ser. Map I-1802-A*, 1986.

Smith, D. E., et al., Topography of the northern hemisphere of Mars from the Mars Orbiter Laser Altimeter (MOLA), *Science*, *279*, 1686-1692, 1998.

Smith, D. E., et al., The global topography of Mars and implications for surface evolution, *Science*, *284*, 1495-1503, 1999.

Soderblom, L., T. Kreidler, and H. Masursky, Latitudinal distribution of a debris mantle on the Martian surface, *J. Geophys. Res.*, *78*, 4117-4122, 1973.

Squyres, S. W., and M. H. Carr, Geomorphic evidence for the distribution of ground ice on Mars, *Science*, *231*, 249-252, 1986.

Squyres, S. W., S. M. Clifford, R. O. Kuzmin, J. R. Zimbelman, and F. M. Costard, Ice in Martian regolith, in *Mars*, edited by H. H. Kieffer, et al., Univ. of Ariz. Press, pp. 523-554, Tucson, 1992.

Tanaka, K. L., Ice-lubricated gravity spreading of the Olympus Mons aureole deposits, *Icarus*, *62*, 191-206, 1985.

Tanaka, K. L., and D. H. Scott, Geological map of the polar regions of Mars, *U. S. Geol. Surv. Misc. Invest. Ser. Map I-1802-C*, 1987.

Thomas, P., S. Squyres, K. Herkenhoff, A. Howard, and B. Murray, Polar deposits of Mars, in *Mars*, edited by H. H. Kieffer, et al., pp. 767-795, Univ. of Ariz. Press, Tucson, 1992.

Thomas, P. C., M. C. Malin, K. S. Edgett, M. H. Carr, W. K. Hartmann, A. P. Ingersoll, P. B. James, L. A. Soderblom, and J. Veverka, North-south geological differences between the residual polar caps on Mars, *Nature*, *404*, 161-164, 2000.

Ward, W.R., Long-term orbital and spin dynamics of Mars, in *Mars*, edited by H. H. Kieffer, eds., pp. 298–320, Univ. of Ariz. Press, Tucson, 1992.

Zuber, M. T., D. E. Smith, J. W. Head, D. O. Muhleman, S. C. Solomon, J. B. Garvin, J. B. Abshire, and J. L. Bufton, The Mars Observer Laser Altimeter investigation, *J. Geophys. Res.*, *97*, 7781-7797, 1992.

J. W. Head III and M. A. Kreslavsky, Department of Geological Sciences, Brown University, Box 1846, Providence, RI 02912. (james_head_iii@brown.edu)

(Received March 27, 2000; revised June 30, 2000;
accepted August 1, 2000.)